Tetragonal Phase in the System ZrO$_2$-Y$_2$O$_3$

V. LANTERI, A. H. HEUER, AND T. E. MITCHELL

Case Western Reserve University
Department of Metallurgy and Materials Science
Case Institute of Technology
Cleveland, OH 44106

AFOSR-TR· 90 0833

Analytical electron microscopy has been used to obtain information on tetragonal (t) ZrO$_2$ in the system ZrO$_2$-Y$_2$O$_3$. Evidence of two tetragonal solid solutions (t and t') has been found in single crystals obtained from skull melting. Of the two, t'-ZrO$_2$ has the higher Y$_2$O$_3$ content and has been described by previous workers as "nontransformable"; it is present in as-grown crystals but is metastable. After annealing at high temperatures (1600°C), t'-ZrO$_2$ decomposes into a mixture of the two equilibrium phases: a low-Y$_2$O$_3$-content t-ZrO$_2$ and a high-Y$_2$O$_3$-content cubic (c) phase, c-ZrO$_2$. The t-ZrO$_2$ appears as precipitate colonies consisting of two twin-related variants in contact along the coherent {101} twin plane.

Precipitates of the high-ZrO$_2$ tetragonal distorted-fluorite phase in the system ZrO$_2$-Y$_2$O$_3$ appear to be quite different from those observed in other well-studied partially stabilized zirconias (Mg-PSZ, Ca-PSZ). In this paper, we discuss the nature of the tetragonal phase in Y$_2$O$_3$-partially stabilized zirconia (Y-PSZ) single crystals. We note that three versions of the phase diagram exist, which differ in detail mainly at the high-ZrO$_2$ region; our work thus also sheds light on the subsolidus phase equilibria in this system.

Scott[4] described a metastable "nontransformable" high-Y$_2$O$_3$-content tetragonal ZrO$_2$ solid solution (t-ZrO$_2$), which he and other workers[5] suggested formed from the cubic ZrO$_2$ solid solution (c-ZrO$_2$) via a displacive phase transformation; the nontransformability relates to its reluctance to undergo the stress-assisted martensitic transformation to monoclinic symmetry found in lower-Y$_2$O$_3$-content t-ZrO$_2$ (Fig. 1). This form of nontransformable t'-ZrO$_2$ is widely encountered in plasma-sprayed Y-PSZ[7-9] and may form only in nonequilibrium situations, as suggested by Scott. For example, t'-ZrO$_2$ was not found by Stubican et al.,[5] who used reactive gels and powders in the experiments that led to their construction of the phase diagram for this system.

Virtually all prior studies of this nontransformable t-ZrO$_2$ have utilized X-ray studies of powders. One of the goals of this study has been the electron microscopy examination of this form of ZrO$_2$ in single crystals. According to Miller et al.,[7] the nontransformable t'-ZrO$_2$ formed in plasma-sprayed Y-PSZ is unstable; if these materials are annealed in the two-phase (t-ZrO$_2$ + c-ZrO$_2$) phase field, t-ZrO$_2$ forms via a diffusion-controlled precipitation reaction and may subsequently transform martensitically to monoclinic symmetry on cooling.

Attention has been given in this work to a single composition (8 wt% Y$_2$O$_3$) in the two-phase field, which should be single phase with cubic symmetry at high temperatures but which, according to the experiments of Miller et al.,[7] should transform to t'-ZrO$_2$ on cooling from high temperature. The stability of t'-ZrO$_2$
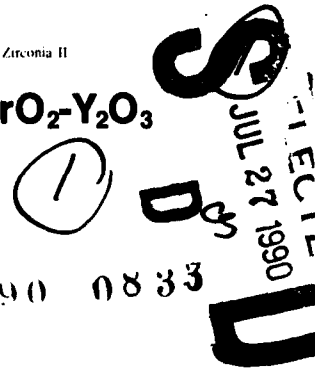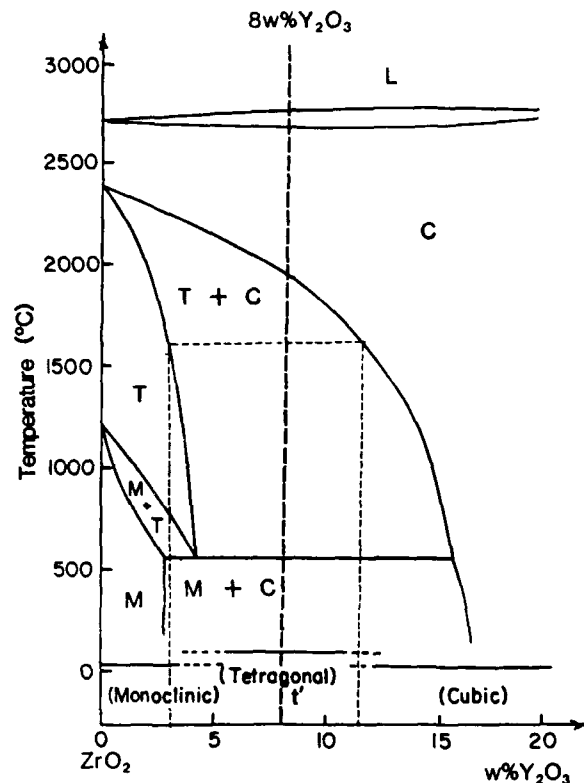
Fig. 1. Phase diagram of the ZrO_2-rich region of the system ZrO_2-Y_2O_3 (Ref. 4).

has been investigated with respect to annealing at high temperatures (1600°C), and the phases present after this heat treatment have been characterized.

Experimental Procedure

As mentioned above, the single-crystal sample used contained 8 wt% Y_2O_3 and was grown by skull melting.* The crystals were opaque and white, a physical appearance characteristic of nonreduced zirconia. For X-ray diffraction, the sample was crushed into fine powder in an agate mortar. Plates (1 by 10 by 10 mm) were annealed in air at 1600°C for 24, 50, and 100 h and quenched by removal from the furnace. The microstructure of the as-received and annealed specimens was characterized by analytical electron microscopy using a Philips EM400T microscope with standard dark-field techniques, supplemented by energy dispersive X-ray analysis (EDX).

Before proceeding to the results, it is appropriate to describe the techniques used to form dark-field images of t-ZrO_2. To distinguish this phase from c-ZrO_2,

*This crystal was furnished by NRL and manufactured by CERES Corp., Waltham, MA. For further information, see Ref. 10.

119

only certain foil orientations can be used, where reflections that are unique to the t phase are present. When transformation from c to t symmetry occurs in this system, whether by precipitation or via a displacive phase transformation, three t variants result, the t c axis being parallel to any of the three original $\langle 100 \rangle_c$ directions. To image all the t variants, the most convenient foil orientation is $\langle 111 \rangle$. Also, t-ZrO$_2$ can be described in terms of either a nonprimitive base-centered unit cell, which in fact is a slightly distorted version of the c fluorite unit cell, or a conventional primitive t unit cell.[11,12] For convenience in this paper, the former C-centered t cell will be used for comparison with the fluorite cell of c-ZrO$_2$.

Results

Figure 2 is a typical [$\bar{1}$11] diffraction pattern of the as-received material. The most intense ("fundamental") reflections are those allowed by both c- and t-ZrO$_2$, whereas the weaker reflections are due to the t phase and have the subscript t. For all $\{1\bar{1}2\}_t$-type reflections to be present in a [$\bar{1}$11] zone axis selected-area diffraction (SAD) pattern, three t variants must be present in the area of foil giving rise to the SAD, each variant giving rise to one $\{1\bar{1}2\}_t$ reflection.[13] It is thus possible to image all the t variants in the dark field using the three $\{1\bar{1}2\}_t$ reflections (see below). X-ray diffraction performed on the as-received specimen showed that only a very small amount of c-ZrO$_2$ was present, indicating that the material contains almost 100% t-ZrO$_2$.

Figure 3 shows dark-field micrographs of the as-received material using the three $\{1\bar{1}2\}_t$ reflections just described. The t-ZrO$_2$ particles imaged in Fig. 3(a) appear to be precipitates $\approx$10 nm thick by $\approx$50 nm long, lying on two $\{101\}$ habit planes. The t-ZrO$_2$ precipitates in Y-PSZ thus appear to be different from t-ZrO$_2$
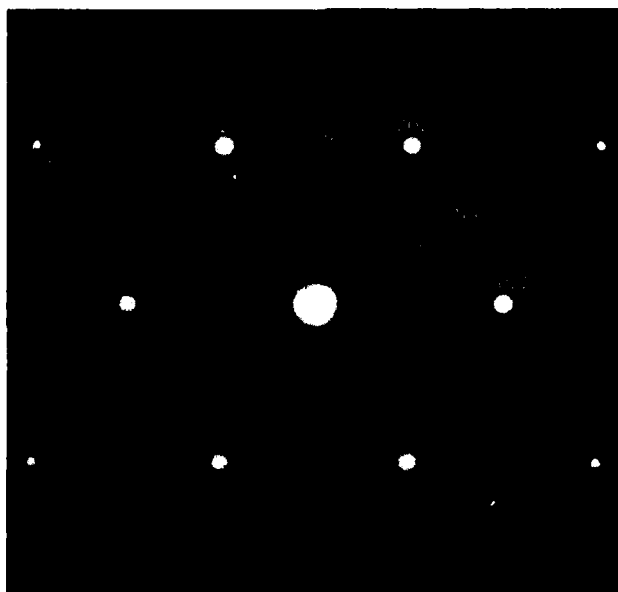

Fig. 2. Diffraction pattern, [$\bar{1}$11] zone axis.

precipitates in Mg-PSZ, where the precipitate/matrix habit plane is invariably {100}, and Ca-PSZ, where the precipitates tend to be equiaxed. Figure 3(b) is obtained by using a second $\{1\bar{1}2\}_t$ reflection in the same area of the foil. A second tetragonal variant is imaged in this case and is also present as well-defined precipitates with a {101} habit plane. The third $\{1\bar{1}2\}_t$ tetragonal reflection (Fig. 3(c)) gives rise to a different microstructure in the same area of the foil — the "matrix" in which the precipitates of Fig. 3(a) and (b), are contained. If the three micrographs are superimposed, all the foil area has been illuminated; it appears that the entire foil area has t symmetry, confirming the X-ray analysis.

It thus appears that the single crystal consists of a t matrix containing t precipitates! We believe that, during the slow cooling that is part of the skull-melting crystal-growth process, a high-temperature displacive transformation from c to t symmetry occurred, giving rise to the t' matrix structure of Fig. 3(c). The precipitates of Fig. 3(a) and (b) are believed to be low-Y_2O_3 t-ZrO_2, which formed via a conventional diffusion-controlled reaction, either from the c phase or from the t'-ZrO_2 itself. The small amount of c-ZrO_2 indicated by the X-ray analysis was not detectable in the area of foil imaged in Fig. 3. It has been suggested[14,15] that the $c \rightarrow t'$ displacive reaction should give rise to antiphase domain boundaries (APBs), which have been imaged by TEM by Bender and Lewis[16] in 3 and 6 wt% Y-PSZ single crystals after laser irradiation, by Chaim et al.[15] in a 12 wt% Y-PSZ polycrystal after suitable heat treatment, and by Michel et al.[17] in 5.4 wt% single crystals. The arrowed features in Fig. 3(c) are also thought to be APBs arising from this transformation.

EDX analysis of the matrix of Fig. 3(c) showed a Y_2O_3 content of ≈ 8 wt%. If, as has been suggested, t-ZrO_2 is a precipitate that formed in a c or t' matrix, then it should have a lower Y_2O_3 content than the parent t' matrix (see Fig. 1). Unfortunately, the small size of the t-ZrO_2 precipitates and the difficulty of distinguishing the precipitates during conventional bright-field imaging prevent confirming this prediction by EDAX analysis. Therefore, we studied further decomposition of the t' matrix during high-temperature (1600°C) annealing, with the expectation that the precipitates would coarsen.

From the phase diagram (Fig. 1), t'-ZrO_2 should decompose into a low-Y_2O_3 t-ZrO_2 solid solution containing ≈ 3 wt% Y_2O_3 plus a c-ZrO_2 solid solution containing ~ 12 wt% Y_2O_3. Dark-field micrographs of the same area of a foil, again obtained with the three $\{1\bar{1}2\}_t$ reflections, are shown in Fig. 4 from a specimen which had been aged 24 h at 1600°C. Figure 4(a) and (b) indicates that the t-ZrO_2 precipitates have grown at the expense of the t' matrix, the precipitates occurring in the form of large "colonies"; each colony actually consists of plates of two twin-related variants. The two variants have different c axes but share a habit plane, which is the coherent twin plane. Small colonies can actually be discerned at the arrowed region of Fig. 3(a); it is clear the colonies coarsen during annealing. The remaining t'-ZrO_2 is imaged in Fig. 4(c); notice that it is located at the periphery of the colonies and has a c axis different from that of the two variants constituting the colony. The t'-ZrO_2 is clearly a minor component, confirming that t'-ZrO_2 is unstable with respect to diffusion at high temperatures. We thus expect the decomposition products of t'-ZrO_2 to be a mixture of equilibrium phases, namely, c-ZrO_2 and the colonies of t-ZrO_2. Such a microstructure can be seen in Fig. 5 from a specimen aged for 50 h at 1600°C. Figure 5(a) is a bright-field micrograph and shows coarse colonies set among c regions. Figure 5(b) is the corresponding dark-field micrograph, taken with a t reflection.

(a)
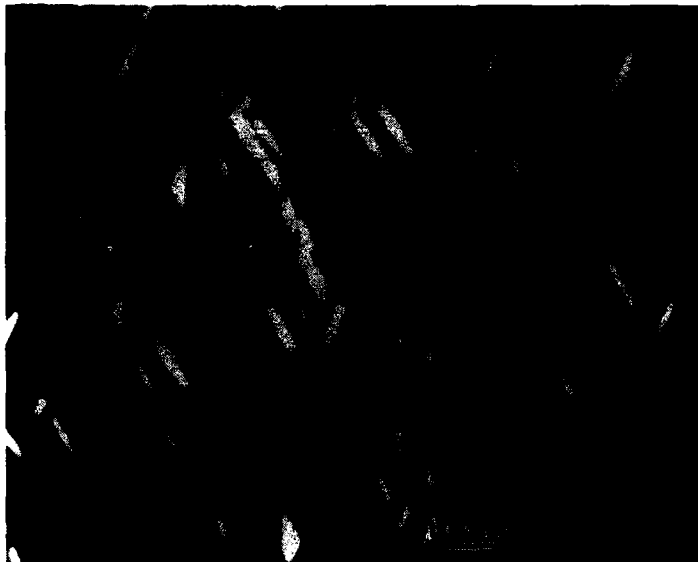
(b)
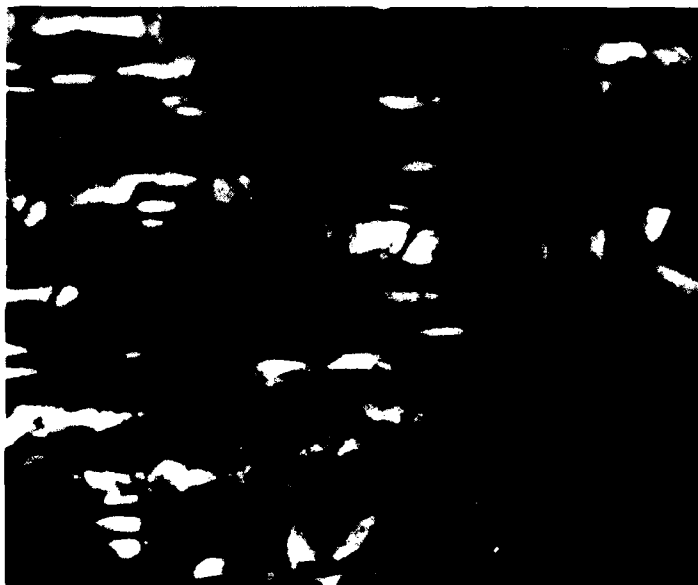
(c)

Fig. 3. Dark-field micrographs of as-received single crystal (8 wt% Y_2O_3).
(a) $g = \bar{1}1\bar{2}$, (b) $g = 211$, and (c) $g = 12\bar{1}$.

Microchemical EDX analysis was performed to compare the Y_2O_3 content of the colonies and the c-ZrO_2. The two spectra are compared in Fig. 6, where it is clear that the c phase is significantly richer in Y_2O_3 than are the t colonies. Quantification of these data revealed a Y_2O_3 content of 4.1 ± 0.1 and $10.6 \pm 0.1\%$ for the colonies and the c-ZrO_2, respectively, close to but not identical with the predictions of Scott's phase diagram (Fig. 1).

The twin relation of variants within the same colony is best illustrated in Fig. 7 from a specimen aged at 1600°C for 100 h; the same features as in Fig. 5 are present, and the coarsening of the tetragonal colonies has progressed further. The selected-area diffraction pattern from one colony shows that only two variants are present. The third variant, which in fact was the original t'-ZrO_2 in the starting material, is not contained in this area of foil. By imaging the colony with the two remaining $\{1\bar{1}2\}_t$ reflections, reverse contrast is observed, showing that the colony indeed contains two twin-related variants.

Discussion

This study has shown evidence of two tetragonal solid solutions, t-ZrO_2 and t'-ZrO_2. These two phases have a quite different microstructure and composition. In the as-received crystal, metastable bulky t'-ZrO_2 is present, while after annealing, the equilibrium t-ZrO_2 precipitates are in the form of colonies. The colony orientation appears to be closely related to the original orientation of the t'-ZrO_2. Within each colony, there are two twin-related variants, whose respective c axes

(a)

(b)

124

(c)

Fig. 4. Dark-field micrographs of specimen aged 24 h at 1600°C:
(a) $\mathbf{g} = \overline{1}1\overline{2}$, (b) $\mathbf{g} = 211$, and (c) $\mathbf{g} = 12\overline{1}$.

are along the **a** and **b** axes of the original t'-ZrO_2. These colonies have also been observed in polycrystalline sintered ceramics with the same Y_2O_3 content[18] and in a 12 wt% Y_2O_3 polycrystal.[15] (In the former material the tetragonal colonies nucleated and grew in a cubic matrix.) The formation of colonies at the expense of the t' matrix, and in c-ZrO_2 grains in a sintered ceramic, and their stability after lengthy annealing suggest that the twin interface within the colonies has an unusually low interfacial energy and that formation of colonies in both t' and c-ZrO_2 minimize lattice strain very effectively. In fact, as the habit plane of the colony is perpendicular to the **a** axis of t'-ZrO_2 and of c-ZrO_2, the "fit" between the t colony and its matrix is very similar in both situations.

Earlier workers also pointed out that t'-ZrO_2 is nontransformable, in the sense that it does not undergo the martensitic transformation to monoclinic symmetry even under stress (e.g., during grinding). However, the t colonies formed from t'-ZrO_2 are also quite stable in that no monoclinic phase was found by X-ray diffraction in crushed specimens that had been annealed for 50 h. This is quite different from what has been observed in other partially stabilized zirconias and is not well understood at this time.

Finally, it is interesting to provide a thermodynamic/kinetic rationale for the existence of two t-ZrO_2 solid solutions in this system. We assume that (i) c-ZrO_2 does form in 8 wt% materials from the melt, (ii) during cooling following skull melting, the cooling history is such that diffusional decomposition to c- and t-ZrO_2, which should occur at $T < 2000°C$ (Fig. 1), does not occur, and (iii) the c-ZrO_2 undergoes a displacive transformation to tetragonal symmetry at some critical

125

(a)

(b)

Fig. 5. Micrographs of specimen aged 50 h at 1600°C: (a) bright field and (b) dark field, **g** = $\overline{1}1\overline{2}$.
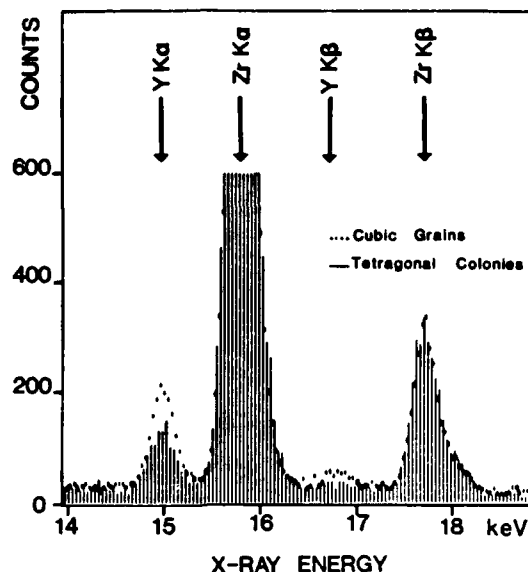
126

Fig. 6. Energy dispersive X-ray spectra of c matrix and t colonies.

temperature T_0. Plausible free energy vs composition curves above and below T_0 are depicted in Fig. 8. Although a two-phase assemblage has the minimum free energy for an 8 wt% material for the situation depicted in Fig. 8(a), supersaturated c-ZrO_2 solid solution will persist until t-ZrO_2 of the equilibrium composition can be nucleated. If cooling below T_0 without nucleation of t-ZrO_2 occurs (Fig. 8(b)), a displacive transformation in an 8 wt% material from supersaturated c-ZrO_2 to supersaturated t'-ZrO_2 can occur and will lower the free energy from G_g to G_t ($\Delta G'$). The solid solution t'-ZrO_2 can further lower its energy by forming t-ZrO_2 of free energy G_t and c-ZrO_2 of free energy G_c for a further energy reduction of $\Delta G''$, but this will be a sluggish transformation, as considerable diffusion is required.

Further study is under way on the mechanism of the displacive $c \rightarrow t'$ transformation and on the variation of T_0 with composition. These experiments should also assist in determining the actual boundaries of the two-phase (c-ZrO_2 + t-ZrO_2) field by using EDX microchemical analysis of the equilibrium microstructures (c-ZrO_2 and colonies of t-ZrO_2).
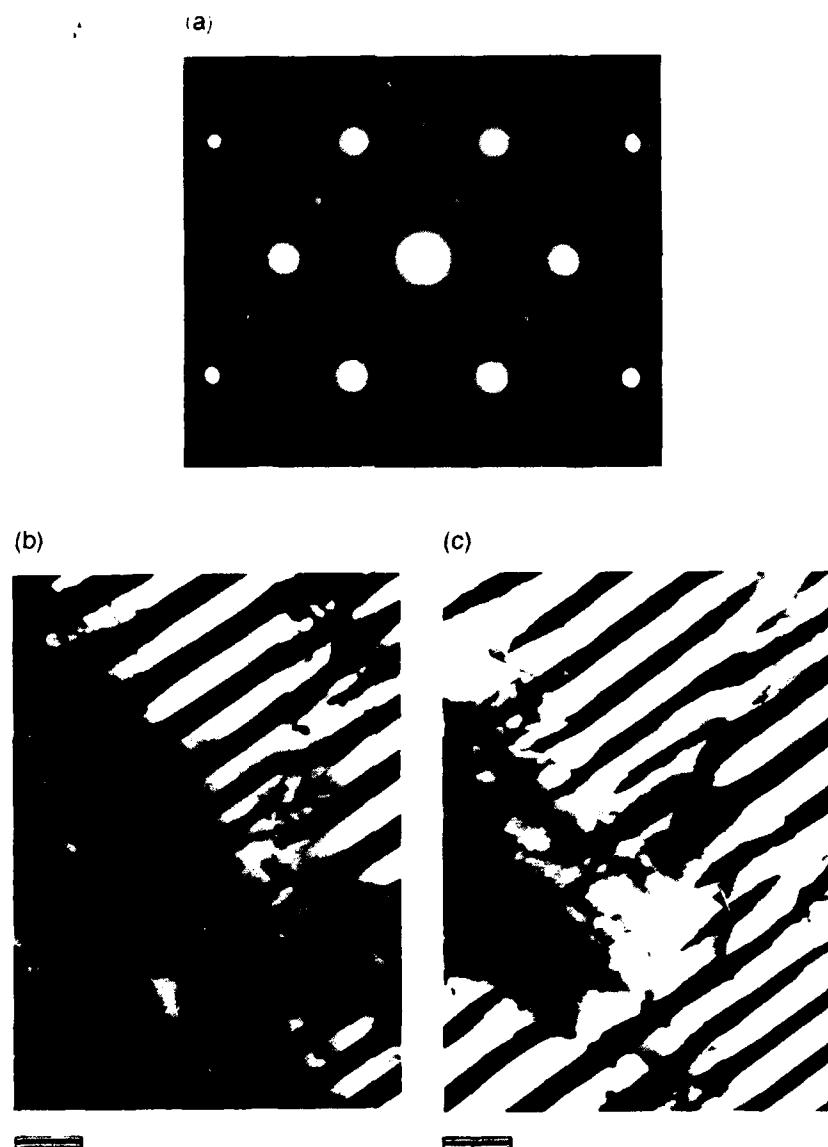
Fig. 7. Specimen aged 100 h at 1600°C: (a) SAD pattern, [$\bar{1}$11] zone axis from one colony, (b) dark-field micrograph, **g** = 11$\bar{2}$, and (c) dark-field micrograph, **g** = 211. The arrows in (b) and (c) point to the same feature. Bar = 500 nm.
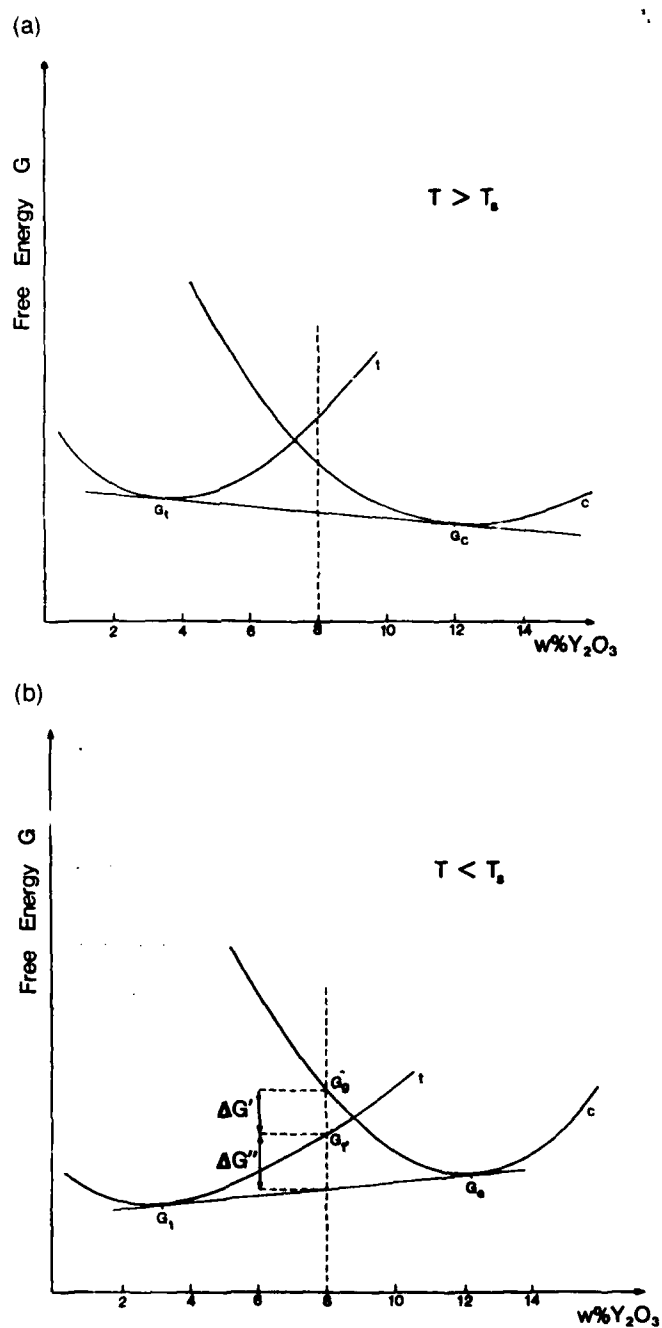
Fig. 8. Free energy vs composition curves: (a) above the critical temperature T_0 and (b) below the critical temperature T_0.

References

[1]R. H. J. Hannink, *J. Mater. Sci.*, **13**, 2487–97 (1978).
[2]D. L. Porter and A. H. Heuer, *J. Am. Ceram. Soc.*, **62** [5–6] 298–305 (1979).
[3]J. M. Marder, T. E. Mitchell, and A. H. Heuer, *Acta Metall.*, **31** [3] 387–95 (1983).
[4]H. J. Scott, *J. Mater. Sci.*, **10** [9] 1527–35 (1975).
[5]V. S. Stubican, R. C. Hink, and S. P. Ray, *J. Am. Ceram. Soc.*, **61** [1–2] 17–21 (1978).
[6]C. Pascual and P. Duran, *J. Am. Ceram. Soc.*, **66** [1] 23–27 (1983).
[7]R. B. Miller, J. L. Smialek, and R. G. Garlick; pp. 241–53 in Advances in Ceramics, Vol. 3. Edited by L. W. Hobbs and A. H. Heuer. The American Ceramic Society, Columbus, OH, 1981.
[8]C. A. Anderson and T. K. Gupta; pp. 184–201 in Advances in Ceramics, Vol. 3. Edited by L. W. Hobbs and A. H. Heuer. The American Ceramic Society, Columbus, OH, 1981.
[9]R. J. Bratton and S. L. Lau; pp. 226–40 in Advances in Ceramics, Vol. 3. Edited by L. W. Hobbs and A. H. Heuer. The American Ceramic Society, Columbus, OH, 1981.
[10]R. P. Ingel; Ph. D. Thesis, The Catholic University of America, Washington, DC (1982).
[11]G. Teufer, *Acta Crystallogr.*, **15** [11] 1187 (1962).
[12]J. Lefevre, *Ann. Chim.*, **8**, 117–49 (1963).
[13]L. H. Schoenlein; Ph. D. Thesis, Case Western Reserve University, Cleveland, OH, 1982.
[14]A. H. Heuer and M. Rühle; this volume, pp. 1–13 .
[15]R. Chaim, A. H. Heuer, and M. Rühle; unpublished results.
[16]B. A. Bender and D. Lewis; private communication.
[17]D. Michel. L. Mazerolles, M Perex, and Y. Jorba; this volume, pp. 131–38.
[18]P. G. Valentine; M.S. Thesis, Case Western Reserve University, Cleveland, OH, 1982.